

Microseismicity detection and seismic ambient noise correlation at the CaMI Field Research Station, Newell County, Alberta

Marie Macquet, Don C. Lawton and J. Helen Isaac

ABSTRACT

We present the continuous seismic data recorded at the CaMI Field Research Station and present results obtained with various methods. We focus here on the microseismicity detection using the STA/LTA method, and on the ambient noise correlation method, applied to imaging and monitoring.

The STA/LTA method is applied on borehole continuous seismic data and detects 10's of thousands of events. The parameters chosen (STA, LTA and threshold) change the absolute number of detected events but the distribution remains the same. We observe an increase in the number of detected events from February to end of March, and the number reduces after end of March. If some days of injection show a large number of detected events, some days without injection also show a large number of events. The frequent human activity (both at the site and in the surroundings) makes difficult to draw conclusions without a better discrimination between human produced events and injection related events.

The ambient noise correlation method is used to produce a near-surface V_S model which is compared with the one obtained with S-wave active source refraction analysis. Ambient noise correlation is also used to try to track the velocity change due to CO₂ injection through the Moving-Window Cross Spectrum analysis applied on the reconstructed Green's function. A last application using this method is the attempt to reconstruct body waves, especially using the downhole continuous seismic data. Preliminary results show a good reconstruction of the body wave when correlating a surface station with downhole stations.

INTRODUCTION

CaMI Field Research Station

The Containment and Monitoring Institute (CaMI) of CMC Research Institutes Inc., in collaboration with the University of Calgary, has developed a comprehensive Field Research Station (FRS) in southern Alberta, Canada, located 200km SE of Calgary (Figure 1). One of the purposes of the CaMI.FRS is to develop early monitoring technologies for potential CO₂ leakage. For that purpose, we are injecting small and controlled amount of CO₂ at shallow depth (Basal Belly River Sandstone Formation - 300m depth, Fig. 1).

Several geophysical and geochemical are installed permanently at the FRS, including:

- a 3D array of 3C geophones (Lawton et al., 2015);
- 3 permanent mounted vibratory sources (Spackman and Lawton, 2017, 2018);

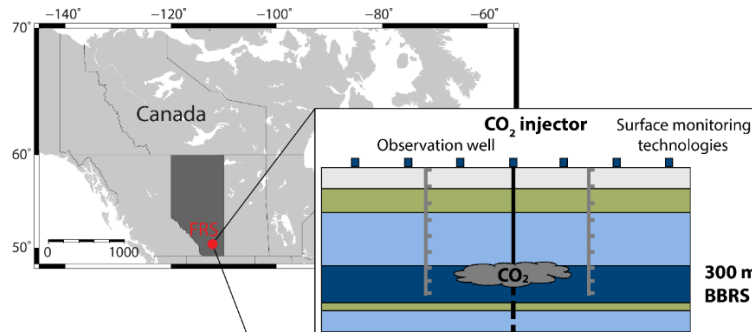


FIG. 1. Location and schematic of the CaMI Field Research Station near Brooks, AB (Canada). BBRS: Basal Belly River Sandstones is the injection target.

- 5km of distributed acoustic sensing (DAS) using straight and helical fiber optical cables deployed in a 1.1km horizontal trench and in 2 observation wells (Gordon and Lawton, 2017, 2018; Hall et al., 2017, 2018; Monsegny et al., 2020);
- a permanent array of 128 electrodes for electrical resistivity tomography buried in the 1.1km trench and in one observation well (Macquet et al., 2020);
- 7 broadband seismic stations (Storke et al., 2018);
- several seismic passive deployments for microseismicity analyses and ambient noise correlation studies (Macquet and Lawton, 2019; Chen et al., 2020; Li et al., 2020; Savard et al., 2020).

In addition to the permanent equipment, several geophysical experiments were and will be conducted at the FRS, including:

- 2D and 3D surface seismic surveys (Isaac and Lawton, 2017);
- Vertical Seismic Surveys (VSP) (Gordon et al., 2016; Hall et al., 2015, 2018; Kolkman-Quinn and Lawton, 2020);
- cross well seismic and electromagnetic surveys (Marchesini et al., 2018, 2019; Alumbaugh et al., 2020);
- punctual electric resistivity tomography surveys (Rippe et al., 2017, 2016);
- magnetometric resistivity surveys (Bouchedda and Giroux, 2016; Bouchedda et al., 2020).

At least two of each were acquired during the baseline time (without injection) to characterized the subsurface and estimate the repeatability of the different methods.

Dataset

In the CCUS projects, seismic data records are widely used to analyse the microseismicity that can be produced by the pressure changes due to CO₂ injection. In addition to standard microseismicity detection, studied here through the STA/LTA method and through other methods such as template matching (Savard et al., 2020), we explore the possibility to use seismic ambient noise correlation for imaging and monitoring (this report, Chen et al. (2020) and Li et al. (2020)).

At the Field Research station, we deployed different surveys to record continuous seismic data. Figure 2 and Table 1 describe the different deployments done over the past few years. In addition to the surface surveys presented here, we record continuously since the end of January on the 24 3C geophones deployed between 191 and 306m depth in the observation well #2 (20m SW from injection well).

Table 1. Summary of the different surveys deployed at the CaMI.FRS for continuous seismic data recording.

Survey Name	Broadband	Oct. 2017	Feb. 2018	Oct. 2018	June 2019	Cont. geophones	borehole
Recording duration	Since Oct. 2014	14days	25 days	7days	25 days	since June 2019	since Jan. 2020
Instruments type	Broadband	geophones	geophones	geophones	geophones	geophones	geophones
Instruments number	7	98	201	10	231	24 then 28	24
Min. aperture	250m	10m	10m	10m	20m	43m	5m
Max. aperture	2.6km	127m	1.1km	43m	1.27km	1.27km	120m
Map on Fig 2	a	b	c	d	e	f	

In his report, we used the continuous borehole geophones data for microseismicity detection through the STA/LTA method; the February 2018 deployment for subsurface imaging through ambient noise correlation; and the broadband data for monitoring through ambient noise correlation. Last part focus on the ability of seismic ambient noise correlation to reconstruct body waves, especially when using the borehole data. The Future work describes the plans we have to use the different other dataset in the next months.

MICROSEISMICITY DETECTION THROUGH STA/LTA

We apply the STA/LTA method (short time average over long time average) on the borehole data. We used a coincidence triggering (i.e. event has to be detected on 8 stations to be considered as a true event) to avoid picking high energy signal that can be produced by instrumental noise and would be different on all stations.

Figure 3 displays the number of events detected by the STA/LTA method on the vertical component of the downhole geophones, using STA=1s, LTA=100 and a threshold of 1.5. We can notice that the Winter time (until roughly end of March) has a larger number of event than the Spring period.

Figure 4 shows a zoom over few days of the comparison between number of detected events (blue) and injection rate (red). In Figure 4.a, we can see a good correlation between number of events and the injection rate on February 27th, but also a day with a large number of events detected but no injection (March 1st). Figure 4.b shows the same variables, for November 2nd. Number of events looks correlated; the events detection seems to start

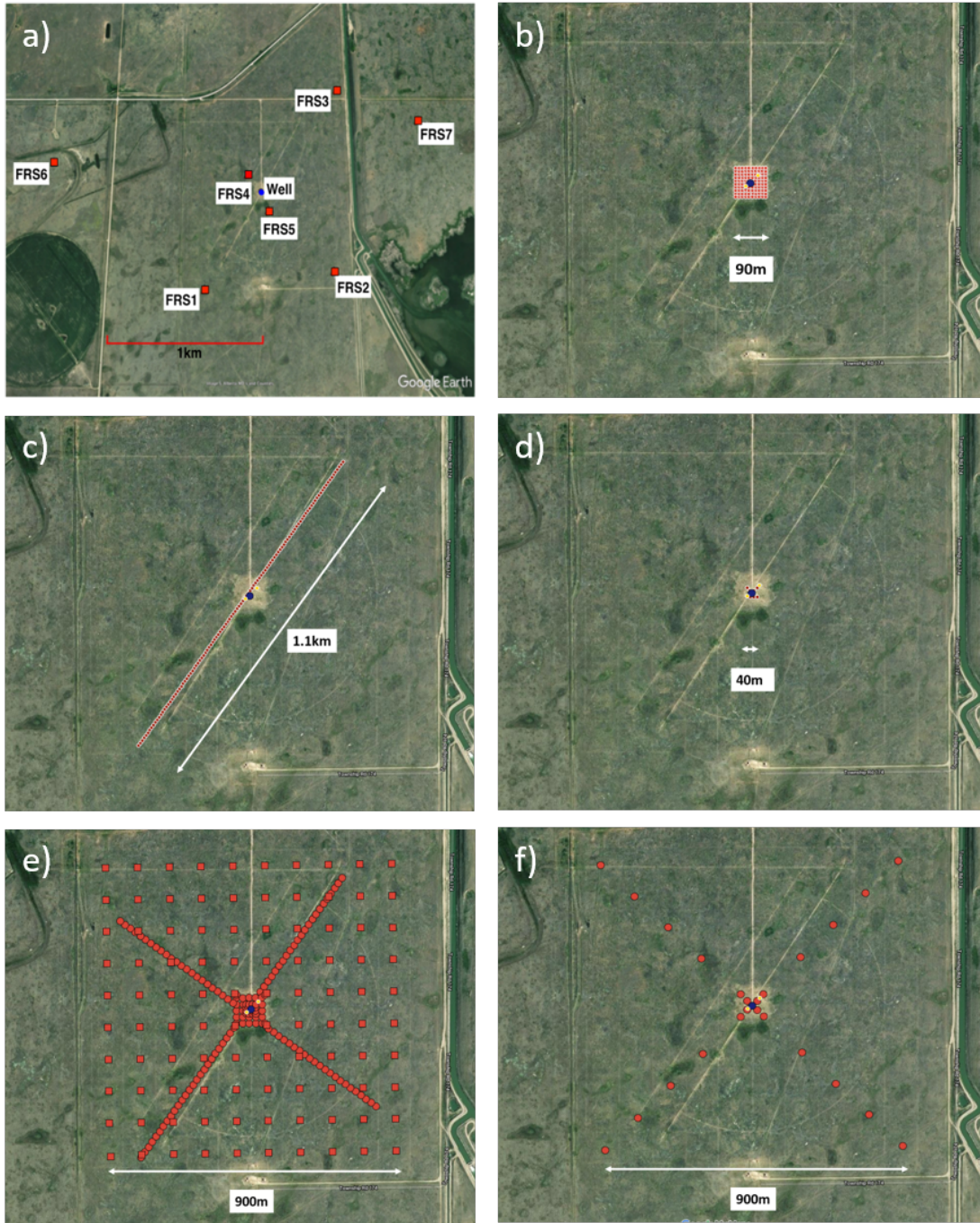


FIG. 2. Different configuration of surveys for continuous seismic data acquisition. Main parameters for each survey are described in Table 1. a) Broadband permanent stations; b) October 2017; c) February 2018; d) October 2018; e) June 2019 and f) since June 2019. Blue dot is the injection well, orange dots are the two monitoring wells.

sooner than the injection, and can be explained by the human activity related noise that probably starts around 8AM. Nevertheless, once the injection starts at 6AM, the number of detected events increases.

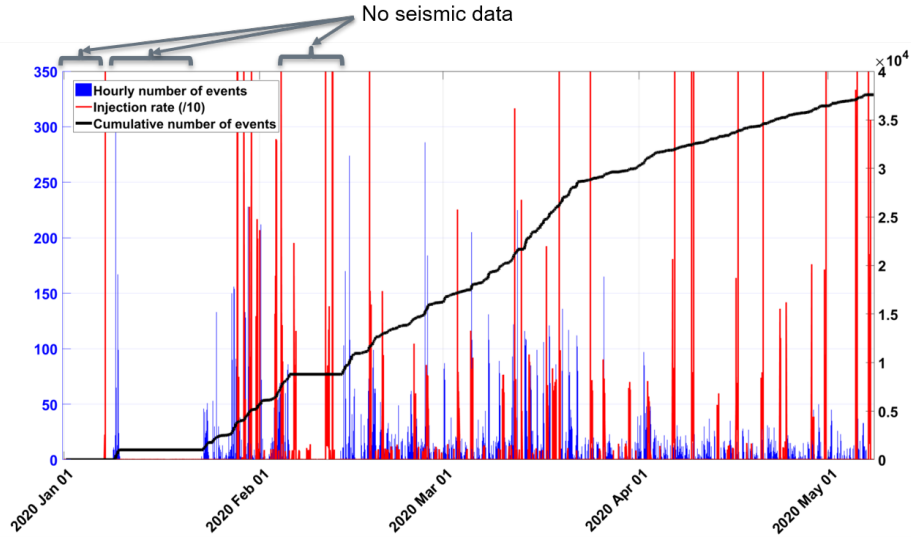


FIG. 3. Events detection and daily injection from January to May 10th 2020.

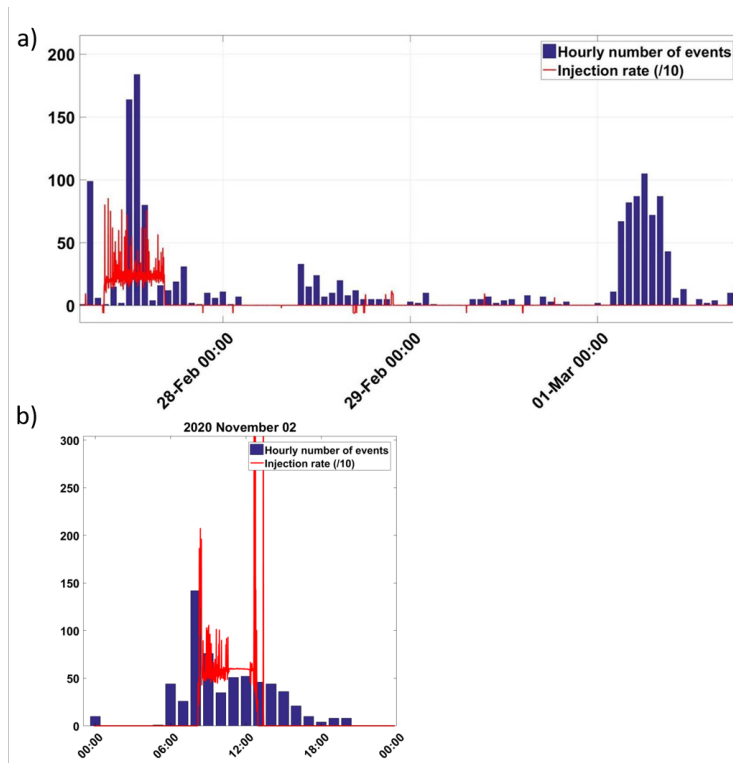


FIG. 4. Detected events through STA/LTA and injection rate. a) February 27th to March 2nd. b) November 2nd.

Conclusions on microseismicity detection

The CaMI.FRS has a great dataset of continuous seismic data, with 24 3C surface geophones and 24 3C downhole geophones, located in the geophysical observation well, 20m away from the injection well. The preliminary work presented here using STA/LTA method shows a huge "seismic" activity at the site. However, the important human activity around and at the site doesn't allow us to draw conclusion on whereas the detected events

are linked or not to the injection. Further analyses, using more complex detection methods (See Savard et al. (2020)), the use of horizontal components and possible machine learning algorithms will be used in the near Future.

COMPARISON BETWEEN S-WAVE SOURCE REFRACTION ANALYSIS AND AMBIENT NOISE TOMOGRAPHY METHOD FOR S-WAVE NEAR SURFACE MODEL

We compare two methods to obtain the S-wave velocity model for the near surface (0-50 m): S-wave source refraction analysis and ambient noise correlation. The two methods were used along the same profile at the CaMI Field Research Station (a pilot site for CO₂ injection located in Alberta, Canada). The average velocity is 265 m/s in the first layer and 910m/s in the second layer using the refraction method. Average velocities are 379 m/s and 763 m/s when using ambient noise correlation method. The bedrock depth is estimated to be at 25 m using refraction analysis and 35 m using the ambient noise correlation technique. The difference can be explained by the trade-off between depth and velocity; the travel times in the first layer are similar in both methods. The two methods have similar results with different advantages: the refraction method gives an accurate and high resolution estimate of bedrock depth as it is based on an inversion of measured travel times on multiple seismic shot records while the ambient noise correlation method has a lower cost as it is based on passive data and can be used at any time.

The mission of the Containment and Monitoring Field Research Station (CaMI.FRS) is to assess and develop monitoring tools for CO₂ storage safety and various geochemical, geochemical and geophysical instruments are deployed on the site (Lawton et al. (2019), Macquet et al. (2019)). The main technique for long-term monitoring of CO₂ behaviour is 4D seismic data analysis (Landrø, 2010). An accurate S-wave velocity model is crucial for multicomponent seismic data processing and analysis. The P-wave velocity model can be obtained through refraction analysis of P-wave data but the S-wave velocity model is more difficult to obtain as shear-sourced S-wave seismic data are rarely acquired. A baseline multi-component survey was acquired in 2014 (Lawton et al., 2019) and a monitor survey will be acquired during the year 2021, after enough CO₂ has been injected for a measurable seismic response (Macquet et al. (2019)). In between these extensive 3D3C acquisitions, several 2D surface and VSP surveys were acquired. In addition to the active survey, we recorded several months of continuous seismic data for induced seismicity detection and ambient noise correlation analysis. We compare two methods of obtaining the near surface S-wave velocity model: S-wave source refraction analysis and ambient noise correlation.

S-wave seismic source

An experimental S-wave seismic survey was acquired at the CaMI.FRS in the summer of 2018. The line was about 1.1 km long and ran SW-NE past the injection well. The seismic source was Echo Seismic Ltd.'s S-wave Envirovibe, which had a base plate generating an S-wave source every 20 m, offset about 5 m from a fixed array of 111 3C geophones spaced 10 m apart. The source sweep was 10-150 Hz but the field data show frequency content diminishing after 50 Hz. The recorded S-wave data are of good quality with clear first breaks (Figure 5).

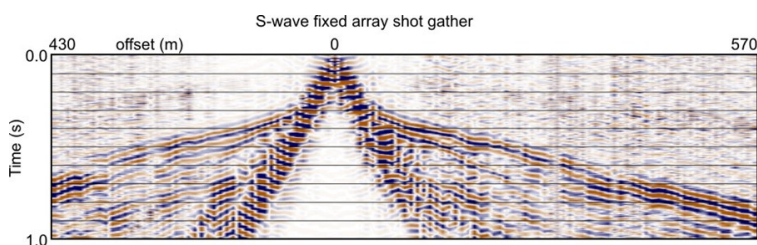


FIG. 5. A shot gather from the S-wave survey. Clear first breaks can be seen with a change in slope at about 60 m offset.

We picked the first breaks and did refraction statics analysis using an offset range of 70-500 m for the second layer in the calculations. The results of this analysis yielded a near-surface S-wave velocity/depth model. Figure 6 shows the smoothed S-wave velocity model from a flat datum of 780 m. The near-surface S-wave low velocity layer is at a depth of 19 to 26.7 m below a flat datum of 780 m, with velocities ranging from 222-288 m/s. The second layer velocities range from 885-930 m/s. The depth of the refractor compares well with the actual bedrock depth of 25.5 below surface elevation of 779.1 m at the injection well location. More details can be found in Isaac and Lawton (2019).

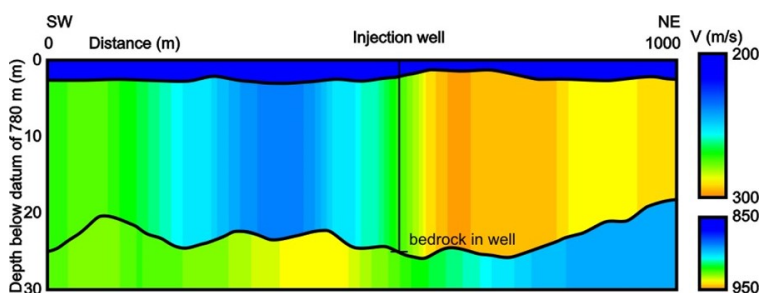


FIG. 6. The depth/velocity model derived from refraction analysis. Near-surface velocities are 222-288 m/s and velocities in the second layer are 885-930 m/s. Depth to the refractor varies from 19-26.7 m. Actual depth of bedrock in the injection well is 26.4 m.

Near surface tomography using ambient noise correlation

In addition to the active seismic data acquired at the CaMI.FRS, several weeks of continuous seismic data were recorded. The dataset used in the present study was acquired in February 2018, using 112 10Hz geophones deployed along the trench, with a receiver spacing of 10 m (Figure 7.a). The whole dataset consists of 25 days of continuous record.

Method

We used the ambient noise correlation method on the continuous dataset. Ambient noise tomography relies on experimental and theoretical validations that the Green's function between two receivers can be derived from the time correlation of a random field recorded by the two receivers (Lobkis and Weaver (2001); Campillo and Paul (2003), Shapiro and Campillo (2004)). As the Green's function is dominated by the fundamental mode of the surface waves for stations located at the surface, group or phase velocity maps can be constructed by correlating the long-duration noise records at the station couples of a seismic array (Shapiro et al. 2005). The dispersion curves obtained from the reconstructed surface

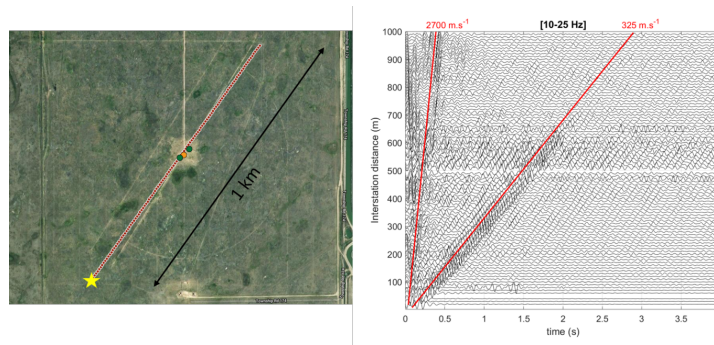


FIG. 7. Virtual shot gather reconstructed with the ambient noise correlation method. (a) Experiment layout; yellow star is the receiver turned into a virtual shot. Orange dot is the injection well location, green dots are the observation well locations. (b) The reconstructed shot gather.

waves can then be inverted for an S-wave velocity model (e.g. Stehly et al. (2009), Macquet et al. (2014)). Since those pioneers' papers, an abundant number of papers have been published using the ambient noise correlation method, in particular at the crustal scale. Indeed, the need of earthquakes or very powerful human sources was removed since the ambient noise correlation method is based on pure noise.

Over the last decade, the ambient noise correlation has also been used at the exploration scale. For example, Mordret et al. (2013) applied the method to the Valhall oil field. The next step was to use the ambient noise correlation for monitoring purposes through monitoring the changes in the reconstructed Green's function. Several studies are focused on monitoring volcano eruptions (Brenguier et al. (2016) per example) while some work has been done on reservoir monitoring (Lehuteur et al. (2018); Obermann et al. (2015)) and the Valhall oil field overburden (Mordret et al. (2014)).

Processing and Green's function reconstruction

The raw signal is first downsampled from 1000Hz to 100Hz and the mean and trend are removed. We applied a standard processing using 1-bit time normalization and spectral whitening (Bensen et al., 2007). The correlations are computed using MSNoise (Lecocq et al., 2014). We correlated the daily correlation for all the pairs of stations. The daily correlations are stacked to obtain the final Green's function approximation. Figure 7.b shows a reconstructed shot gather. It represents the correlation between one station (yellow star on Figure 7.a) and all the other stations. The yellow station is turned into a virtual source. The causal and acausal parts are stacked here.

We can see the surface wave (Rayleigh wave, as we use the vertical components) with a velocity of 325 m/s. We interpret the faster wave to be a body wave. We compute the cross correlation between all the pairs of stations and obtain a starting dataset of 4098 paths for the next steps.

Dispersion curves

We sum the causal and acausal part of the correlation and use the frequency-time analysis method (FTAN, Levshin et al. (1989)) to compute the group velocity dispersion curves between each pair of stations. Some selection criteria were applied:

- A signal to noise ratio superior to 5 to keep only the high-quality correlations (Figure 8.a). We remove 900 paths using a threshold of 5 (Figure 8.c).
- A wavelength superior to 1 (Luo et al., 2015). The number of final measurements ranges from 2600 at 5 Hz to 3100 at 20 Hz (Figure 8.c).

We choose to keep the outliers' measurement (rather than applying a threshold on the standard deviation for example) as the number of measurements is large and the frequency histogram shows a Gaussian distribution (Figure 8.b).

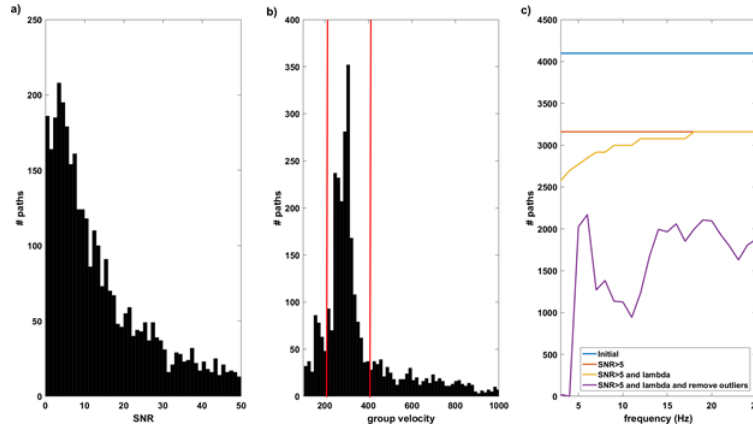


FIG. 8. a) SNR distribution. b) Group velocity distribution. Red lines represent the mode velocity ± 100 m/s. c) Number of correlations kept as a function of the QC criteria.

2D group velocity

We regionalize the dispersion curves computed between each pair of stations using the method of Barmin et al. (2001). The model m is estimated by minimizing the penalty function:

$$S(m) = (G_m - d)^T C_d^{-1} (G_m - d) + m^T Q_m \quad (1)$$

where d is the data vector, G is the forward operator, C_d is the data covariance and Q_m is the regularization matrix.

The regularization matrix is based on the lateral smoothing and the damping, which are determined using L-curves. The cell size is 10 m, and the number of paths in the middle of the model can reach up to 1000 depending on the considered frequency. We produce a 1D group velocity model following the trench for each frequency (Figure 9).

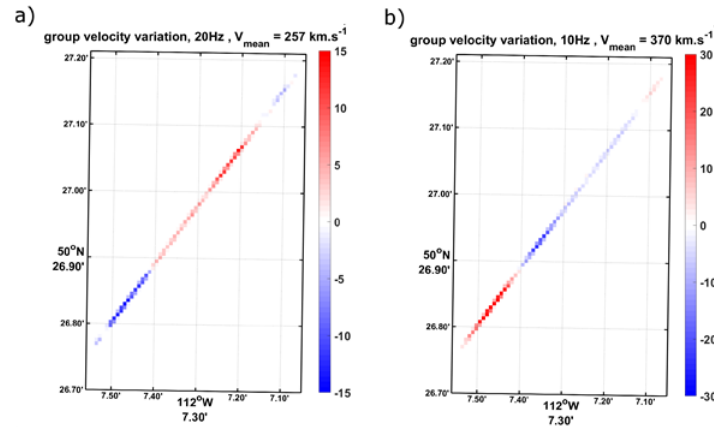


FIG. 9. Group velocity variation along the trench. a) At 20 Hz. b) At 10 Hz. The mean group velocity is indicated on the top of the map. 20 Hz data are more sensitive to shallower part than 10 Hz data.

The 1D maps are combined to obtain the 2D group velocity presented in Figure 10.

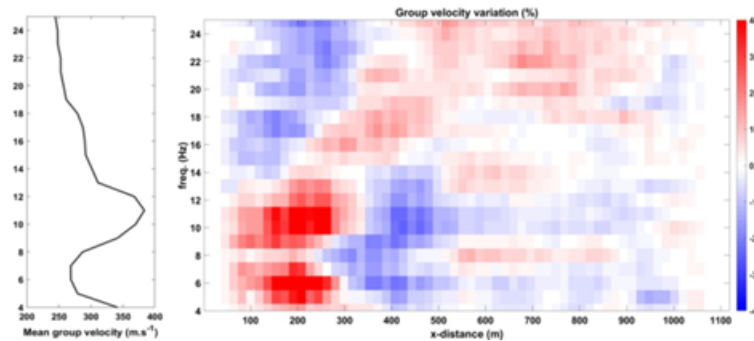


FIG. 10. Group velocity variation (right) compared to average velocity of the specific period (left).

We can observe that on Figure 10:

- The velocities are increasing with depth;
- At shallow depths the velocity is lower in the SW part than in the NE part of the trench;
- At deeper depths the velocity is higher in the SW part than in the NE part on the trench.

These observations are consistent with the S-wave velocity model obtained by the refraction method.

Local dispersion curve inversion

We extract the local dispersion curve for each cell of the 2D model and invert it to get the local VS model for that location. We use SRFPython package developed by Lehujeur

et al. (2018). It uses a Monte-Carlo inversion approach, using the forward modelling computation developed by Herrmann (2013). We use the boundaries presented in Table 2 for the model space. It is based on the velocity model obtained in the previous section but keeping wide boundaries to avoid putting too strong constraints on the inversion and to allow a higher degree of freedom. 12 independent Markov chains are running in parallel until 500 models are retained and we keep the 2500 best models of the 6000 selected ones.

Table 2. Prior boundaries of uniform probability distribution.

Layer #	Bottom depth range (m)	V_S range (m/s)
1	0.2-10	100-300
2	20-40	200-400
3	infinite half space	700-1500

Figure 11 shows the results for one dispersion curve. Figure 11.a shows the retained 2500 models, color plotted as a function of their likelihood and Figure 11.b are their associated dispersion curves. The final model is the average of the 50th percentile (grey curve).

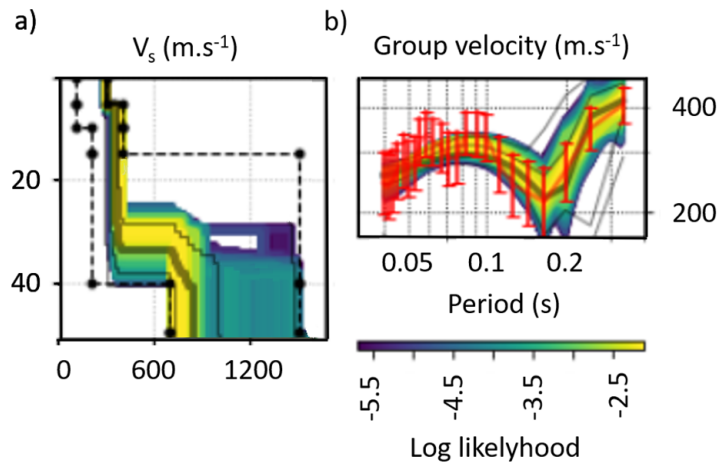


FIG. 11. Inversion of a local dispersion curve. a) 2500 best models, colors corresponding to log-likelihood value. Dotted black lines are the prior boundaries described in Table 1. Thick grey is the final model. Thin grey lines indicate the 1st, 16th, 84th and 99th percentiles. b) Corresponding associated dispersion curves (fundamental mode of Rayleigh wave). Red is the observed one, with associated errors, and the thick grey corresponds to the final inverted model.

2D V_S model

We run the inversion described in the previous subsection for each local dispersion curve and we combine the 1D S-wave models obtained to get the 2D section. Figure 12 is the result of the inversion.

The general pattern is consistent with the model obtained using S-wave source refraction analysis. The shallow layer shows S-wave velocity going from 334 to 395 m/s (higher than that derived from the S-wave source refraction analysis method) with a low velocity zone in the SW part. The deeper layer shows velocity going from 707 to 820 m/s (lower than that derived from the S-wave source refraction analysis method) with a high velocity

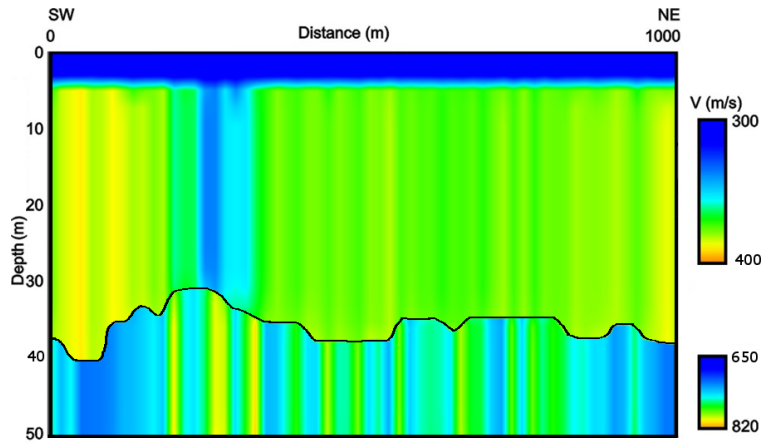


FIG. 12. Inverted VS model along the trench.

zone in the SW part. The bed rock depth is going from 30.1 to 38.3 m depth, deeper than the model obtained with the refraction analysis. We can note the low velocity layer at the surface that allows the model to absorb the absence of topography in the inversion process.

Comparison between the two models

Figure 13 shows the comparison of the depth of the bedrock and the S-wave velocity in the 2 layers for both methods. Uncertainties for the ambient noise correlation are computed using the 16th and 84th percentiles of the 2500 best selected models.

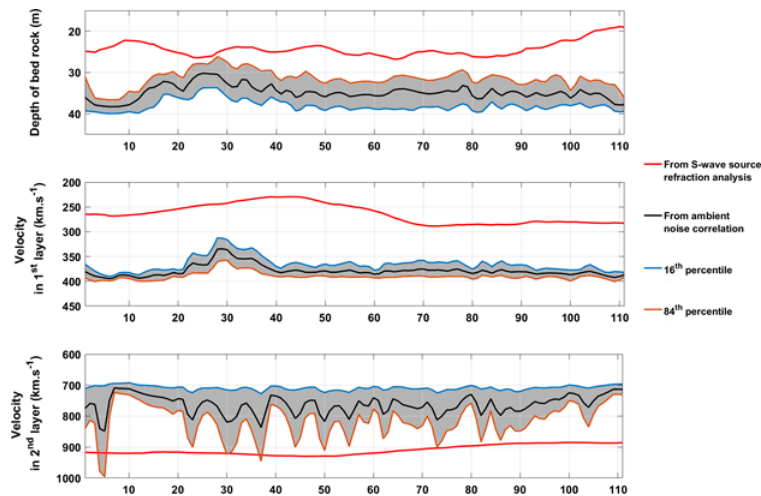


FIG. 13. Comparison between results from S-wave source refraction analysis and ambient noise correlation for the depth of the bed rock and the S-wave velocity in the two layers. Errors for the ambient noise correlation method are added in grey as the range between the 16th and 84th percentiles.

The ambient noise correlation over-estimates the depth of the be rock (Fig. 13.a). Even if the prior boundaries allow the bedrock depth to be between 15 and 40 m (Table 2), the final model remains close to the upper boundaries (final model between 30.1 and 38.3 m deep). The averaged uncertainty is ± 3.2 m. The ambient noise correlation also over-estimates the velocity in the first layer. The velocity in this layer is well constrained (av-

eraged uncertainty is ± 12 m/s) with an average of 378 m/s even if the prior boundaries allows the exploration of models with velocity as low as 200 m/s (Table 2). Despite low uncertainties, the velocities obtained using the ambient noise correlation are higher than the ones obtained with the S-wave source refraction analysis (an average of 378 m/s compared to 263 m/s). The velocities obtained for the 2nd layer with the ambient noise correlation are lower than the ones obtained with the refraction analysis. Even with the possibility of models with velocities as high as 1500 m/s (Table 2), the results remain close to the lower boundary (average of 762 m/s with an uncertainty of ± 50 m/s). The difference can be explained by the well-known trade-off between velocity and depth; the deeper bedrock obtained with the ambient noise correlation is compensated by higher velocity, however the travel times used in both methods are similar.

Conclusions on near surface models

We used two different methods to estimate the near surface-S-wave velocity. They show similar results, but each has its advantages and inconveniences. The first method using the S-wave source gives a profile of the bedrock based on refraction analysis. The second method based on ambient noise tomography has a lower resolution as it is based on passive acquisition. However the cost is lower than using an active source, can be done at any time, and the method applied to a 2D deployment can be used to produce a 3D near surface S-wave velocity model at low cost.

MONITORING USING AMBIENT NOISE CORRELATION

Method

The MSNoise package, developed by Lecocq et al. (2014) implements the Moving-Window Cross Spectrum analysis (MWCS, first introduced by Ratdomopurbo and Poupinet (1995), also called doublet method). The method basically compares the daily short-windows cross correlation (here the daily one) and a reference correlation (here the average over the whole period). An example of daily and reference correlations between station FRS3 and FRS4 are shown on Figure 14.

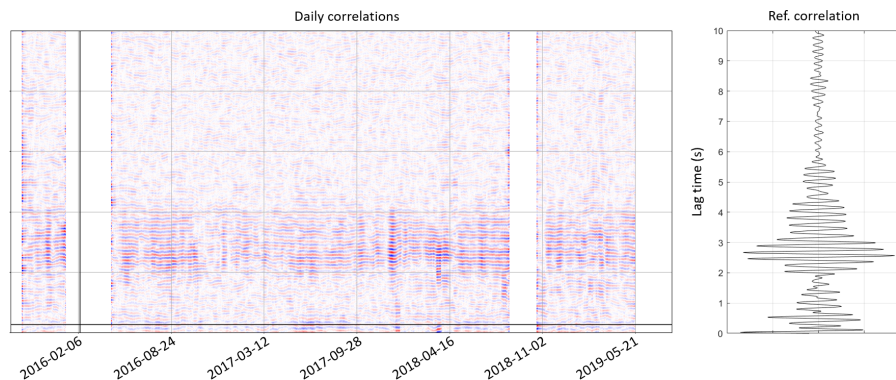


FIG. 14. Left: 4 years of daily correlations between two broadband stations (FRS3 and FRS4). Right: stacked correlation.

For a detailed theory of the method, readers can refer to Clarke et al. (2011). We apply the MWCS on the 4 years of data we have on 7 broadband stations (Figure 2.a). Figure 15

shows the average velocity variation observed for all pairs of stations. The analysis is done in the [0.1-1]Hz frequency range, in the [0.5-5]s time window. Figure 15.a shows the daily velocity variation (in black) as well as the smoothed curve (over 40 days, in red). We can clearly see a good correlation between the smoothed curve and the average temperature (Figure 15.b). Figure 15.c shows the daily CO₂ injection, with the periods of injection highlighted in green. They seem to correspond to periods of velocity variation decreasing (Figure 15.a).

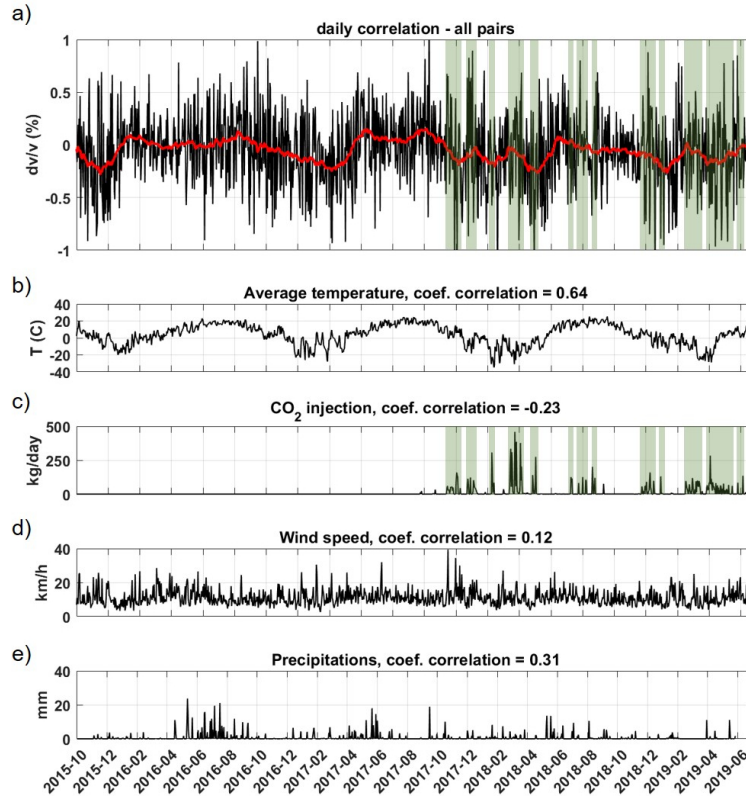


FIG. 15. a) Black : Averaged velocity variation obtained from daily cross correlation. Red : 40-days smoothing curve . b) Average daily temperature. c) Daily injection. d) Wind speed at 2m high. e) Rain precipitation.

Conclusions on monitoring trough ambient noise correlation

The main challenge at the Field Research Station is the weak amount of CO₂ that is planned to be injected in order to simulate a leakage (Macquet et al., 2019). Less than 500kg/day will induce relatively small plume size (compare to large-scale field) and small variation in elastic parameters. As the use of ambient noise can be highly affected by environmental changes, a very careful analysis of the system is required to fully understand which parameters influences the Green's function reconstruction and so which parameters can be the cause of the observed velocity variation. The effect of the seasonal temperature is clearly visible on the velocity variation curves but we also suspect an effect of the CO₂ injection. Further analysis is required to confirm the first observations and be able to associate observed velocity variation to the correct parameters (weather changes or CO₂ injection). The goal being to determine if the ambient noise correlation technique can be used to detect the subsurface changes due to a small amount of injected CO₂.

The monitoring work will be updated with the last dataset of continuous seismic data recorded on the broadband array (Figure 16). Since June 2019, seismic continuous acquisition was also done on 24 geophones (Figure 2.f), and the downhole geophones are also continuously recording since January 2020. They will be added to this study. In 2020, the CO₂ injection increases, making the CO₂ injection effects detection using ambient noise correlation theoretically easier.

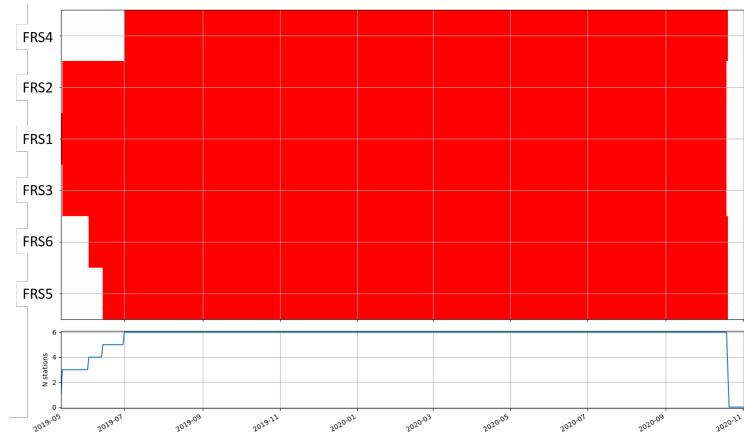


FIG. 16. Broadband stations availability to be added to this study.

BODY WAVES RECONSTRUCTION - PRELIMINARY WORK

Figure 17 shows different studies done using seismic ambient noise correlation with the surface CaMI.FRS continuous data that were able to reconstruct the body wave.

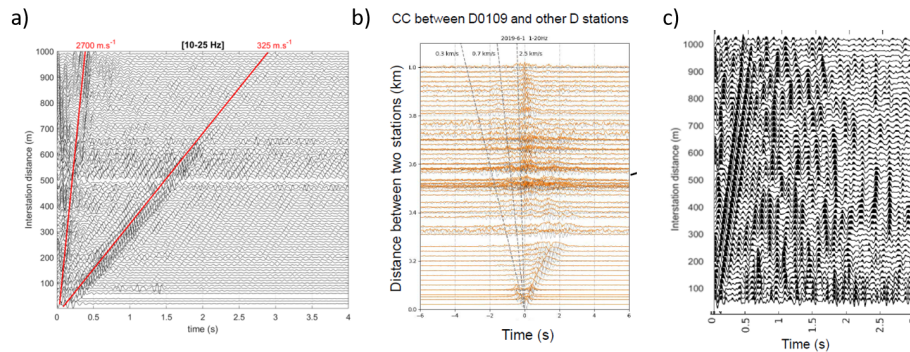


FIG. 17. Body wave reconstruction using seismic ambient noise correlation. a) Using February 2018 dataset (Fig 2.c), from this study. b) Using Summer June 2019 dataset (Fig 2.e), from Li et al. (2020). c) Using Summer June 2019 dataset (Fig 2.e), from Chen et al. (2020).

Since January 2020, we also record continuous seismic data on the downhole geophones. We extracted a subset of 5 stations (F0802, F0010 and C0404 at the surface, G6 and G18 on the observation well), and correlate the continuous ambient noise between all of them. Figure 18.a shows the schematic location of the stations, and Figure 18.b shows the causal part of the reconstructed Green's function. We can see the reconstructed surface wave between A-B and A-C (B and C being at the surface), and the reconstructed body wave between A-D and A-E (D and E being in the well).

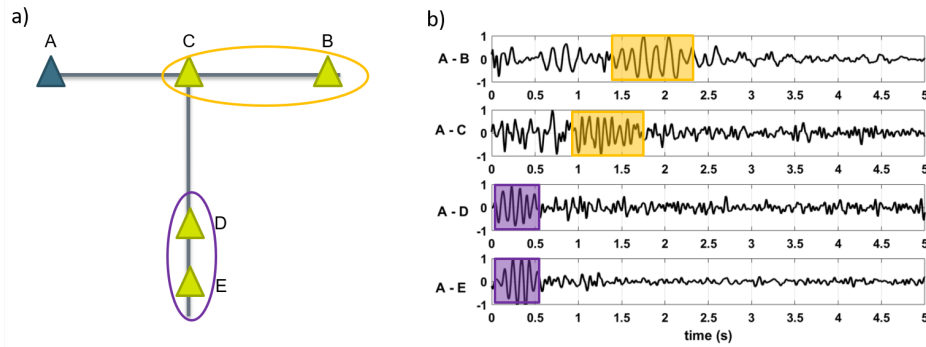


FIG. 18. a) Schematic location of the 5 stations used for the test. b) Reconstructed Green's function between A and the 4 other stations.

We will extend this preliminary work to the whole dataset (24 3C stations at the surface, and 24 3C stations downhole) and test the possibility to use the reconstructed body wave for imaging and monitoring.

CONCLUSIONS AND FUTURE WORK

Continuous seismic data are extremely valuable in CCS projects (but also EOR, fracking...). They allow the study of the microseismicity that can be due to CO₂ injection, and this information is one of the first tool to attest of the caprock integrity and reservoir conformance. We apply a very standard and simple STA/LTA method that show the complexity of the events detected at the FRS. Methods such as template matching were also used (Savard et al., 2020). Next step will be to automatically discriminate between human produced events and injection related ones, and understand the behaviour of the reservoir and the effect of the pressure changes on the microseismicity.

We show the possibilities brought by the ambient noise correlation method, for imaging and monitoring. Unfortunately, the type of geophones (10Hz) used at the FRS doesn't give us the frequency range needed to image at the reservoir depth. However, a near surface model is extremely important for active seismic processing. In October 2020, we deployed an array of 35 Fairfield nodes (5Hz) that will allow to image deeper than the 10Hz geophones deployment did.

The preliminary results on monitoring through ambient noise correlation show encouraging results on the broadband data. We will add the last dataset to the results (broadband from May 2019 to now), and apply the same method to the X-array of geophones (Figure 2.f). The results of the MWCS method will be compared to the results obtained through the Coherence of Correlated Waveforms (CCW) method which is based on attenuation changes in the medium (Delouche et al. (2019), Voisin and Delouche (2019)).

Ambient noise correlation is widely based on surface wave or coda analysis; extraction of body waves in the Green's function is now the next step (Figure 17). We will use the continuous borehole seismic data to improve the body wave reconstruction, and use them for imaging and monitoring.

Even with the recent progresses (through body wave recovery for example) the resolution of the imaging through ambient noise correlation will unlikely catch up with the abilities of the active seismic. Nevertheless, it can still be used as a cheap early detection method, that can be refined through active survey if needed.

ACKNOWLEDGEMENTS

We thank CaMI JIP and CREWES sponsors for their financial support. We also gratefully acknowledge support from NSERC (Natural Science and Engineering Research Council of Canada) through the grants CRDPJ 461179-13 and CRDPJ 543578-19. This research was undertaken thanks in part to funding from the Canada First Research Excellence Fund. We thank Thomas Lecocq for developing and distributing the MSNoise codes. We appreciate the collaboration with Echo Seismic Ltd. for acquisition of the S-wave seismic data, and the generous contribution by Halliburton/Landmark for SeisSpace seismic data processing software. We thank Malcolm Bertram for his valuable help on the field. We thank all the persons that took part to the various fieldwork.

REFERENCES

- Alumbaugh, D., Um, E., Marchesini, P., Wilt, M., Nichols, E., Vasco, D., Daley, T., and Key, K., 2020, Joint Use of crosswell EM and seismic for monitoring CO₂ storage at the CaMI.FRS : baseline surveys and preliminary results : CaMI.FRS JIP Workshop.
- Barmin, M. P., Ritzwoller, M. H., and Levshin, A. L., 2001, A fast and reliable method for surface wave tomography: *Pure App. Geophys.*, 1351–1375.
- Bensen, G. D., Ritzwoller, M. H., Barmin, M. P., Levshin, A. L., Li, F., Moschetti, M. P., Shapiro, N. M., and Yang, Y., 2007, Processing seismic ambient noise data to obtain reliable broad-band surface wave dispersion measurements: *Geophysical Journal International*, **169**, 1239–1260.
- Bouchedda, A., Giroux, B., Macquet, M., and Lawton, D., 2020, Downhole magnetometric resistivity modelling and inversion on unstructured mesh as a tool for interpreting monitoring data, application at the cami.frs: CaMI.FRS JIP Workshop.
- Bouchedda, A., and Giroux, B., 2016, MMR measurements at the Field Research Station, Alberta, 2016: CAMI Research Report, **1**.
- Brenguier, F., Rivet, D., Obermann, A., Nakata, N., Boué, P., Lecocq, T., Campillo, M., and Shapiro, N., 2016, 4-D noise-based seismology at volcanoes: Ongoing efforts and perspectives: *Journal of Volcanology and Geothermal Research*, **321**, 182–195.
- Campillo, M., and Paul, A., 2003, Long-range correlations in the diffuse seismic coda: *Science*, **299**, No. 5606, 547–549.
- Chen, Y., Gu, Y. J., Sacchi, M. D., Li, T., Macquet, M., Gilbert, H., and Lawton, D. C., 2020, Passive seismic imaging and monitoring using ambient noise body waves, CaMI Field Research Station, Newell County, Alberta, Canada: CaMI.FRS JIP workshop.
- Clarke, D., Zaccarelli, L., Shapiro, N., and Brenguier, F., 2011, Assessment of resolution and accuracy of the moving window cross spectral technique for monitoring crustal temporal variations using ambient seismic noise: *Geophysical Journal International*, **186**, No. 2, 867–882.
- Delouche, E., Voisin, C., and Stehly, L., 2019, Seismic precursors in central Italy using coherence of correlated waveforms: *AGUFM*, **2019**, S24A–08.
- Gordon, A., and Lawton, D. C., 2017, Zero offset VSP processing of fiber optic cable (DAS) and geophone array at the CaMI Field Research Station: CREWES Research Report, **29**.

- Gordon, A., and Lawton, D. C., 2018, Walk away VSP processing of DAS and geophone data at the CaMI Field Research Station, Newell county, Alberta: CREWES Research Report, **30**.
- Gordon, A., Lawton, D. C., and Eaton, D. W., 2016, VSP azimuthal travel time analysis at the Field Research Station near Brooks, Alberta: CREWES Research Report, **28**.
- Hall, K. W., Bertram, K., Bertram, M., Innanen, K., and Lawton, D., 2018, Crewes 2018 multi-azimuth walk-away VSP field experiment: CREWES Research Report, **30**.
- Hall, K. W., Isaac, J. H., Wong, J., Bertram, K. L., Bertram, M. B., Lawton, D. C., Bao, X., and Eaton, D., 2015, Initial 3C-2D surface seismic and walkaway VSP results from the 2015 Brooks SuperCable experiment: CREWES Research Report, **27**.
- Hall, K. W., Lawton, D. C., Daley, T., Freifeld, B., and Cook, P., 2017, Source distance and source effort on DAS data: CREWES Research Report, **29**.
- Herrmann, R. B., 2013, Computer programs in seismology: An evolving tool for instruction and research: *Seismological Research Letters*, **84**, No. 6, 1081–1088.
- Isaac, J. H., and Lawton, D. C., 2017, A summary of surface seismic reflection data acquired at the Field Research Station near Brooks, Alberta: CREWES Research Report, **29**.
- Isaac, J. H., and Lawton, D. C., 2019, Seismic studies of the near-surface at the CaMI Field Research Station, Newell County, Alberta: CREWES Research Report, **31**.
- Kolkman-Quinn, B., and Lawton, D., 2020, Time-lapse VSP at the CaMI Field Research Station, Newell County, Alberta, Canada: CaMI.FRS JIP workshop.
- Landrø, M., 2010, 4D seismic, *in* *Petroleum Geoscience*, Springer, 489–514.
- Lawton, D. C., Bertram, M., and Bertram, K. H. K., 2015, New approaches to seismic monitoring at the Brooks Field Research Station: CREWES Research Report, **27**.
- Lawton, D. C., Dongas, J., Osadetz, K., Saeedfar, A., and Macquet, M., 2019, Development and analysis of a geostatic model for shallow CO₂ injection at the Field Research Station, Southern Alberta, Canada: *Geophysics and Geosequestration*. Cambridge University Press, Cambridge, **280**, 296.
- Lecocq, T., Caudron, C., and Brenguier, F., 2014, MSNoise, a Python package for monitoring seismic velocity changes using ambient seismic noise: *Seismological Research Letters*, **85**, No. 3, 715–726.
- Lehuteur, T., Vergne, J., Schmittbuhl, J., Wigone, D., Le Chenadec, A., and EstOF Team, 2018, Reservoir imaging using ambient noise correlation from a dense seismic network: *Journal of Geophysical Research-Solid Earth*, **123**, No. 8, 6671–6686.
- Levshin, A., Yanocskaya, T. B., Lander, A. V., Bukchin, B. G., Barmin, M. P., Ratnikova, L. I., and Its, E. N., 1989, *Seismic surface waves in a laterally inhomogeneous earth*: edited by V. I. Keilis-Borok, Springer, New York.
- Li, T., Gu, Y. J., Lawton, D. C., Gilbert, H., Savard, G., Macquet, M., and Innanen, K., 2020, Monitoring CO₂ injection at the CaMI Field Reserach Station using noise source migration: CaMI.FRS JIP workshop.
- Lobkis, O. I., and Weaver, R. L., 2001, On the emergence of the Green's function in the correlations of a diffuse field: *The Journal of the Acoustical Society of America*, **110**, No. 6, 3011–3017.
- Luo, Y., Yang, Y., Xu, Y., Xu, H., Zhao, K., and Wang, K., 2015, On the limitations of interstation distances in ambient noise tomography: *Geophysical Journal International*, **201**, No. 2, 652–661.
- Macquet, M., Lawton, D., Rippe, D., Schmidt-Hattenberger, C., Osadetz, K., Maidment, G., and Bertram, M., 2020, Semi-continuous ERT monitoring at the CaMI Field Reserach Station using noise source migration: CaMI.FRS JIP workshop.

- Macquet, M., and Lawton, D. C., 2019, Ambient noise correlation study at the CaMI Field Research Station, Newell County, Alberta, Canada: CMC annual report, vol.4.
- Macquet, M., Lawton, D. C., Saeedfar, A., and Osadetz, K. G., 2019, A feasibility study for detection threshold of CO₂ at shallow depths at the CaMI Field Research Station, Newell County, Alberta, Canada: Petroleum Geoscience, petgeo2018–135.
- Macquet, M., Paul, A., Pedersen, H., Villaseñor, A., Chevrot, S., Sylvander, M., and Wolyniec, D., 2014, Ambient noise tomography of the Pyrenees and the surrounding regions: inversion for a 3-D Vs model in the presence of a very heterogeneous crust: *Geophysical Journal International*, **199**, No. 1, 402–415.
- Marchesini, P., Daley, T. M., and Nihei, K., 2019, Updates on crosswell seismic tomographic surveying at CaMI-FRS: Containment and Monitoring Institute and CMC Research Institutes Subscriber workshop.
- Marchesini, P., Daley, T. M., Wilt, M., Nichols, E., Um, E., and Cook, P., 2018, Baseline data for crosswell seismic and electromagnetics at CaMI: Containment and Monitoring Institute and CMC Research Institutes Subscriber workshop.
- Monsegny, J., Hall, K., Trad, D., and Lawton, D., 2020, Least squares migration DAS to geophone transfrom, application at the CaMI Field Research Station, Newell County, Alberta, Canada: CaMI.FRS JIP workshop.
- Mordret, A., Landès, M., Shapiro, N., Singh, S., and Roux, P., 2014, Ambient noise surface wave tomography to determine the shallow shear velocity structure at Valhall: depth inversion with a neighbourhood algorithm: *Geophysical Journal International*, **198**, No. 3, 1514–1525.
- Mordret, A., Landès, M., Shapiro, N., Singh, S., Roux, P., and Barkved, O. I., 2013, Near-surface study at the valhall oil field from ambient noise surface wave tomography: *Geophysical Journal International*, **193**, No. 3, 1627–1643.
- Obermann, A., Kraft, T., Larose, E., and Wiemer, S., 2015, Potential of ambient seismic noise techniques to monitor the St. Gallen geothermal site (Switzerland): *Journal of Geophysical Research: Solid Earth*.
- Ratdomopurbo, A., and Poupinet, G., 1995, Monitoring a temporal change of seismic velocity in a volcano: Application to the 1992 eruption of Mt. Merapi (Indonesia): *Geophysical Research Letters*, **22**, No. 7, 775–778.
- Rippe, D., Schmidt-Hattenberger, C., and Lettow, H., 2017, Electrical resistivity tomography measurements at the Field Research Station near Brooks, Alberta, Canada (September 19 – September 22, 2016): CaMI Research Report, **2**.
- Rippe, D., Strom, A., and Schmidt-Hattenberger, C., 2016, Electrical resistivity tomography baseline repeat at the Field Research Station near Brooks, Alberta, Canada (September 26 – October 4, 2017): CaMI Research Report, **1**.
- Savard, G., Gilbert, H., Macquet, M., Lawton, D., and Osadetz, K., 2020, Microseismicity detection and observations at the CaMI Field Research Station, Newell County, Alberta Canada: CaMI.FRS JIP Workshop.
- Shapiro, N., and Campillo, M., 2004, Emergence of broadband Rayleigh waves from correlations of the ambient seismic noise: *Geophysical Research Letters*, **31**, No. 7.
- Spackman, T. W., and Lawton, D. C., 2017, Seismic monitoring with continuous seismic sources: CREWES Research Report, **29**.
- Spackman, T. W., and Lawton, D. C., 2018, Processing and analysis of data recorded from a buried permanent seismic source: CREWES Research Report, **30**.
- Stehly, L., Fry, B., Campillo, M., Shapiro, N., Guilbert, J., Boschi, L., and Giardini, D., 2009, Tomography of the Alpine region from observations of seismic ambient noise: *Geophysical Journal International*, **178**, No. 1, 338–350.

Storke, A., Kendall, M., Kendall, R., Horleston, A., and Goble, D., 2018, Broadband monitoring at FRS - baseline results: Containment and Monitoring Institute and CMC Research Institutes Subscriber workshop.

Voisin, C., and Delouche, E., 2019, Deep crustal fluids monitoring of the central apennines with ambient seismic noise: AGUFM, **2019**, S21E–0545.